Simple Feedback Control of Cockroach Running

J. Schmitt

Oregon State University, Corvallis, Oregon
schmitjo@engr.orst.edu

Summary. The spring loaded inverted pendulum model (SLIP) has been shown to accurately model sagittal plane locomotion for a variety of legged animals. Tuned appropriately, the model exhibits passively stable periodic gaits using either fixed leg touchdown angle or swing-leg retraction protocols. In this work, we investigate the relevance of the model in insect locomotion and develop a simple feedback control law to enlarge the basin of stability and produce stable periodic gaits for both the point mass and rigid body models. Control is applied once per stance phase through appropriate choice of the leg touchdown angle. The control law is unique in that stabilization is achieved solely through direct observation of the leg angle and body orientation, rather than through feedback of system positions, velocities, and orientation.

1 Introduction

The spring loaded inverted pendulum (SLIP) [1, 2, 3, 4] has emerged as a template of locomotion dynamics in the vertical plane for a large number of animals. In the model, the combination of legs animals use during each stance phase is idealized as a single effective leg represented by an elastic spring. Experimental research on animal locomotion has shown that running animals use multiple legs as one [5], and that the resulting body motion is well represented by this simple template [1, 2, 6, 7]. For suitable model parameters, both the rigid body and point mass models produce self-stabilizing periodic gaits, with or without the inclusion of simple feedforward control methodologies [8, 9, 10].

Much of the previous research on the SLIP model has utilized a fixed angle leg reset policy, where the leg touchdown angle remains constant for each stance phase. While this leg touchdown protocol produces stable periodic gaits for the point mass and rigid body models, the basin of stability for the rigid body model remains quite small and stability is only achieved for suitably tuned model parameters [8]. Additionally, use of a similar fixed angle leg reset protocol in a three dimensional spatial SLIP model produces only unstable periodic gaits [11]. In this work, we investigate the performance of

the two dimensional SLIP model in modeling insect locomotion and, looking forward to developing simple stabilizing controllers for the spatial SLIP model, construct a simple feedback control law to expand the basin of stability for periodic orbits of both the point mass and rigid body SLIP models.

The paper is structured as follows. In Sect. 2, we briefly review the rigid body vertical plane SLIP formulation of [8]. While we primarily focus on the point mass model, extensions to motions of the rigid body model are also considered in Sect. 4.2. In Sect. 3, we investigate the stability of periodic gaits of the SLIP model with model parameters similar to those of the cockroach *Blaberus discoidalis*. We find that the fixed angle leg reset policy utilized in previous works produces predominantly unstable periodic gaits for these model parameters. These results, in conjunction with the stability results of the spatial SLIP model for a similar leg touchdown protocol, prompt an investigation into the stability properties of alternate leg touchdown protocols. Specifically, we begin by analyzing a leg touchdown protocol that places the next leg down at the same angle, relative to the inertial frame, that the previous leg was lifted. Neglecting gravity during the stance phase, we show that such a protocol produces neutrally stable period two as well as period one orbits. Since one of the eigenvalues of the period one orbits is negative one, continuity arguments suggest that leg placement protocols between these extremes will produce stable periodic gaits. We therefore introduce a simple, adaptive leg touchdown angle control law in Sect. 4.1 that connects both this leg touchdown protocol as well as the fixed angle leg reset policy, and show that the control law improves the stability properties of periodic gaits. We briefly consider the stability of periodic orbits of the rigid body model under a similar control law in Sect. 4.2, and numerically show that while inclusion of this control law produces stable gaits, periodic gaits are only necessarily achieved by incorporating delay feedback control into the control law.

2 Review of SLIP Model Formulation

The SLIP model, illustrated in Fig. 1, consists of a rigid body of mass m and moment of inertia I. A pair of legs are attached at a frictionless pin joint P in the body, displaced a distance d from the center of mass, where d can take either sign. While the SLIP model has primarily been used in investigating the motions of larger animals, in this work we examine its relevance in insect locomotion, in particular the locomotion of the cockroach *Blaberus discoidalis*. Cockroaches run in an alternating tripod gait, with three legs down during each stance phase. Experiments have shown that the forces produced by these legs during the stance phase are well represented by a single effective leg. Since the mass of the legs of the insect comprise less than 6% of the total mass, we therefore model the tripod of legs by a single, massless effective leg represented by a linear, elastic spring of nominal length l.

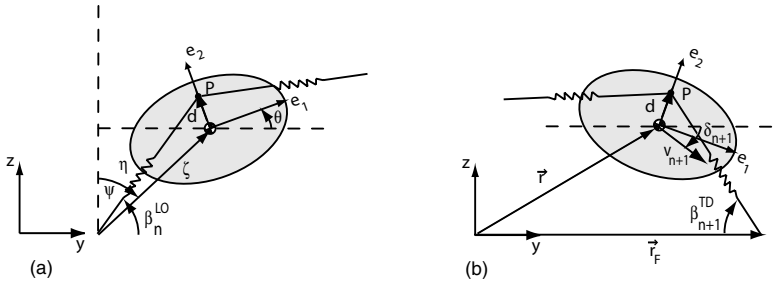

Fig. 1. SLIP rigid body model formulation, illustrating coordinate systems and relevant quantities at (**a**) leg lift-off and (**b**) leg touchdown

If both legs are attached at the same point P in the body, a full stride consists of a stance and flight phase, since left and right stance phases are indistinguishable. The stance phase begins when the leg, extended at its nominal length l, touches the ground at an angle β_n^{TD} with respect to the inertial frame. Superscripts of TD and LO denote values at touchdown and lift-off respectively, whereas subscripts identify the specific stance phase. The foot placement remains fixed during the stance phase and is represented by a moment free pin joint. Under the influence of gravity and its own momentum, the body moves forward in the y direction during the stance phase, compressing and extending the elastic leg. When the leg returns to its nominal length, it is lifted from an angle β_n^{LO} with respect to the inertial frame and a flight phase ensues. Simple ballistic dynamics govern the flight phase, and the next stance phase begins when the leg touches the ground, placed at an angle β_{n+1}^{TD} with respect to the inertial frame. While feedforward control is required to place each leg in anticipation of the next stance phase, no energy is required to move the leg to the prescribed position since the leg has no mass. As a result, the system is passive and energy is globally conserved, since no impacts or impulses occur.

The equations of motion for the stance phase are derived in [8] and summarized here, implemented with a linear spring leg:

$$\begin{aligned} m\ddot{\zeta} &= m\zeta\dot{\psi}^2 - mg\cos(\psi) - k(1-\frac{l}{\eta})(\zeta + d\cos(\theta+\psi)) \\ 2m\zeta\dot{\zeta}\dot{\psi} + m\zeta^2\ddot{\psi} &= mg\sin(\psi) + k(1-\frac{l}{\eta})d\zeta\sin(\theta+\psi) \\ I\ddot{\theta} &= k(1-\frac{l}{\eta})d\zeta\sin(\theta+\psi) \end{aligned} \tag{1}$$

where η, ζ, ψ, θ, and k denote the leg length, distance from the foot placement to the center of mass, angle ζ makes with the vertical inertial axis, body rotation, and spring stiffness respectively. The flight phase dynamics are governed by simple ballistic dynamics which may be integrated to yield

$$y(t) = y^{LO} + \dot{y}^{LO}t,\ z(t) = z^{LO} + \dot{z}^{LO}t - \frac{1}{2}gt^2,\ \theta(t) = \theta^{LO} + \dot{\theta}^{LO}t\ . \quad (2)$$

The composition of the stance and flight phase dynamics result in a piecewise-holonomic system. While systems with piecewise-holonomic constraints can display asymptotic stability [12], they are often best described in terms of partial asympototic stability. In these cases, the corresponding periodic motions typically exhibit some neutral eigendirections (with eigenvalue = 0 or Floquet multiplier = 1) often associated with conserved quantities or symmetries such as energy conservation or rotational invariance. As in previous analyses for the conservative horizontal and vertical plane models [8, 13], perturbations to stable gaits in the direction of the eigenvector(s) of these conserved quantities or symmetries do not grow nor decay, but result in the attainment of a new gait.

3 Periodic Gaits, Stability and Control

Many prior SLIP model analyses focus on gait properties for a fixed angle leg reset model, where the leg is reset to its original touchdown angle at the beginning of each stance phase. For model parameter ranges consistent with larger animals, these studies illustrate the ability of the model to produce passively stable gaits. While we initially examine gaits produced for a fixed angle leg reset model with parameters set to those typical of the roach *Blaberus discoidalis*, we subsequently investigate simple feedback control laws that prescribe the leg touchdown angle and enhance stability.

In all cases, simulations are developed and performed using the Runge-Kutta integrator ode45 available in Matlab. As in previous work [8, 14, 15], we determine periodic orbits and their stability through use of a Poincaré map [16], with a Poincaré section defined at the instant of leg touchdown. Fixed points of the mapping represent periodic gaits in the continuous system, and are identified by a Newton-Raphson iteration. As illustrated in Fig. 1, we simplify the stability analysis through the definition of our Poincaré map in terms of variables of a new coordinate frame $(v, \delta, \theta, \dot{\theta}, \beta)$, where v is the center of mass velocity, δ is the velocity heading angle measured clockwise from the inertial horizontal axis, θ is the body rotation and $\dot{\theta}$ is the angular velocity.

Stability of fixed points of the mapping is determined by examining the eigenvalues of the linearization of the Poincaré map about the fixed point. If any eigenvalue is greater than unity the periodic orbit is unstable and if all non-unity eigenvalues remain within the unit circle, the periodic orbit is stable.

3.1 Fixed Angle Leg Reset Gaits

We begin by investigating the point mass SLIP model with parameters similar to those of the cockroach *Blaberus discoidalis*: spring stiffness (k) of 20 N/m,

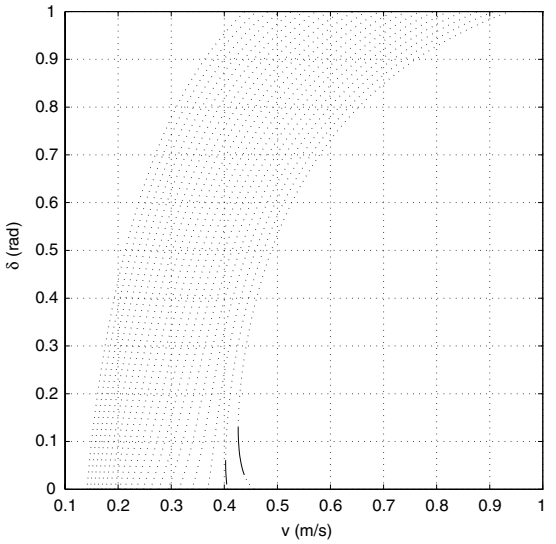

Fig. 2. Point mass SLIP gait families $(v_n^{TD}, \delta_n^{TD})$ for $\beta_n^{TD} = 1.1 - 1.3$. Gait stability is indicated by *dotted* and *solid lines* for unstable and stable gaits respectively. Model parameters used in calculating the gaits are similar to those of *Blaberus discoidalis*, as described in the text. Gait families for increasing β_n^{TD} are obtained as one moves from *right* to *left* in the plot

leg length (l) of 0.015 m, body mass (m) of 0.0025 kg, and a leg touchdown angle (β_n^{TD}) between $1.1 - 1.3$ radians. These parameter values are chosen to produce reasonable leg compressions (less than 50%) during the stance phase, as well as to match experimental stride length and frequency results [17]. While the theoretical results neglect gravity during the stance phase so that angular momentum is conserved, gravity is included in both stance and flight phases in all simulations conducted in this work. In this section, we consider only the point mass SLIP model with $d = 0$; extensions to the rigid body model with $d \neq 0$ and an adaptive control law are presented in Sect. 4.2.

Using Newton-Raphson routines in conjunction with the model simulation, we obtain a one parameter family of periodic gaits, depending upon the body touchdown velocity, v. The gait family is initially obtained for a nominal value of $\beta_n^{TD} = 1.20$, which best matches the experimental stride length and frequency results. Gait families for values of $\beta_n^{TD} = 1.1 - 1.3$ are subsequently obtained to see if changes in gait stability occur for these alternate values, even though stride length and frequency results do not necessarily match those observed experimentally. As illustrated in Fig. 2, almost all periodic gaits obtained over this range of leg touchdown angles are unstable. A small range of stable periodic gaits exist for leg touchdown values between $1.1 - 1.11$, although the minimum touchdown speeds obtained in these instances exceed the preferred operating speed of 0.25 m/s of *Blaberus discoidalis*.

3.2 Alternate Leg Angle Touchdown Protocols

The stability properties of the SLIP model with parameters similar to those of *Blaberus discoidalis*, in conjunction with the instability results of the fixed angle leg reset policy in the three dimensional spatial SLIP model, prompt an investigation into alternate leg touchdown protocols. A problem with the fixed angle leg reset policy is the propensity for the model to trip. During each flight phase, the body must attain a height sufficient to place the next leg down at the constant touchdown angle. Many initial conditions produce gaits that do not satisfy this condition, leading to gaps in the mapping where no periodic gaits can exist, as found in [8]. A simple means of eliminating these gaps is to place the next leg down at the previous leg liftoff angle, $\beta_{n+1}^{TD} = \beta_n^{LO}$. Even in the absence of a flight phase, a model utilizing this leg touchdown protocol on a level surface will not stumble, although the forward velocity may be insufficient to compress the elastic spring and move the body forwards past the foot placement point.

Properties of Period Two Gaits with $\boldsymbol{\beta_{n+1}^{TD} = \beta_n^{LO}}$

Implementing a leg touchdown protocol where the new leg touchdown angle equals the previous leg lift-off angle primarily produces asymmetric period two gaits, $\beta_{n+2}^{TD} = \beta_n^{TD} \neq \beta_{n+1}^{TD}$, although period one gaits also exist, due to the symmetry of leg touchdown and lift-off angles in such gaits, $\beta_n^{TD} = \beta_n^{LO}$. We construct a Poincaré map, through the use of conservation laws, to determine necessary conditions for periodic orbits, as well as stability properties of those orbits. Analytically, as in previous studies [11, 8], we assume that leg forces dominate gravity forces during the stance phase. As in [8], we use a mixed approximation in computing the stance map, where we concurrently neglect the effect of gravity during stance to retain conservation of angular momentum, but retain the effect of gravity in computing the velocity mapping to enforce energy conservation. The variations in the leg angle swept during stance, $\Delta\psi$, therefore reduce to those examined in the lateral leg spring model [14, 13], and the analyses conducted therein apply.

We compute the touchdown velocity mapping directly from energy conservation, with the zero potential energy level defined at the initial touchdown height as

$$\frac{m(v_n^{TD})^2}{2} = \frac{m(v_{n+2}^{TD})^2}{2} + mgl(\sin(\beta_{n+2}^{TD}) - \sin(\beta_n^{TD})) \tag{3}$$

$$v_{n+2}^{TD} = \sqrt{(v_n^{TD})^2 + 2gl(\sin(\beta_n^{TD}) - \sin(\beta_{n+2}^{TD}))}\,. \tag{4}$$

We compute the velocity heading angle mapping using conservation of linear momentum, conservation of angular momentum and conservation of energy. Since the next leg touchdown angle equals the previous leg lift-off angle in

this protocol, conservation of energy between the lift-off and touchdown conditions necessarily yields $v_{n+1}^{TD} = v_n^{LO}$ and $v_{n+2}^{TD} = v_{n+1}^{LO}$. Conservation of linear momentum during the flight phase

$$v_{n+1}^{TD}\cos(\delta_{n+1}^{TD}) = v_n^{LO}\cos(\delta_n^{LO}) \tag{5}$$

$$v_{n+2}^{TD}\cos(\delta_{n+2}^{TD}) = v_{n+1}^{LO}\cos(\delta_{n+1}^{LO}) \tag{6}$$

therefore yields $\delta_{n+1}^{TD} = -\delta_n^{LO}$ and $\delta_{n+2}^{TD} = -\delta_{n+1}^{LO}$. Since gravity is neglected during stance, angular momentum is conserved during each stance phase

$$ml^2 v_n^{TD}\sin(\beta_n^{TD} - \delta_n^{TD}) = ml^2 v_n^{LO}\sin(\beta_n^{LO} + \delta_n^{LO}) \tag{7}$$

$$ml^2 v_{n+1}^{TD}\sin(\beta_{n+1}^{TD} - \delta_{n+1}^{TD}) = ml^2 v_{n+1}^{LO}\sin(\beta_{n+1}^{LO} + \delta_{n+1}^{LO})\,. \tag{8}$$

Utilizing the relationships for the velocities, velocity heading angles and leg touchdown protocol developed above, however, we find that the magnitude of angular momentum remains constant across all stance phases for this protocol

$$ml^2 v_n^{LO}\sin(\beta_n^{LO} + \delta_n^{LO}) = ml^2 v_{n+1}^{TD}\sin(\beta_{n+1}^{TD} - \delta_{n+1}^{TD}) \tag{9}$$

$$ml^2 v_{n+1}^{LO}\sin(\beta_{n+1}^{LO} + \delta_{n+1}^{LO}) = ml^2 v_{n+2}^{TD}\sin(\beta_{n+2}^{TD} - \delta_{n+2}^{TD})\,. \tag{10}$$

As a result, we find

$$ml^2 v_{n+2}^{TD}\sin(\beta_{n+2}^{TD} - \delta_{n+2}^{TD}) = ml^2 v_n^{TD}\sin(\beta_n^{TD} - \delta_n^{TD}) \tag{11}$$

such that the velocity heading angle map can be expressed as

$$\delta_{n+2}^{TD} = \beta_{n+2}^{TD} - \sin^{-1}\left(\frac{v_n^{TD}}{v_{n+2}^{TD}}\sin(\beta_n^{TD} - \delta_n^{TD})\right)\,. \tag{12}$$

Stance phase geometry and the leg touchdown protocol produce a relationship for the leg touchdown angle mapping as

$$\begin{aligned}\beta_{n+2}^{TD} &= \beta_{n+1}^{LO} = \pi - \Delta\psi_2 - \beta_{n+1}^{TD} \\ &= \pi - \Delta\psi_2 - (\pi - \Delta\psi_1 - \beta_n^{TD}) \\ &= \Delta\psi_1 - \Delta\psi_2 + \beta_n^{TD}\end{aligned} \tag{13}$$

where $\Delta\psi_1$ and $\Delta\psi_2$ represent the leg angle swept during the first and second stance phase respectively. The full period two Poincaré map is therefore comprised by equations (4), (12), and (13), and a periodic orbit for this mapping requires $\Delta\psi_1 = \Delta\psi_2$. Ignoring gravity, the formulas for each $\Delta\psi$ can be constructed from conservation of angular momentum and energy during the stance phase, as in [14], to yield

$$\Delta\psi_1 = \int_{\zeta_{b1}}^{l} \frac{2v_n^{TD} l \sin(\beta_n^{TD} - \delta_n^{TD}) d\zeta}{\zeta\sqrt{((v_n^{TD})^2 - k/m(\zeta - l)^2)\zeta^2 - l^2(v_n^{TD})^2 \sin^2(\beta_n^{TD} - \delta_n^{TD})}} \quad (14)$$

$$\Delta\psi_2 = \int_{\zeta_{b2}}^{l} \frac{2v_{n+1}^{TD} l \sin(\beta_{n+1}^{TD} - \delta_{n+1}^{TD}) d\zeta}{\zeta\sqrt{(a - k/m(\zeta - l)^2)\zeta^2 - l^2(v_{n+1}^{TD})^2 \sin^2(\beta_{n+1}^{TD} - \delta_{n+1}^{TD})}} \quad (15)$$

$$a = (v_{n+1}^{TD})^2 + 2gl(\sin(\beta_{n+1}^{TD}) - \sin(\beta_n^{TD})) \quad (16)$$

where ζ_{b1}, ζ_{b2} are the largest positive roots of the equation(s)

$$ml^2(v_n^{TD})^2 \sin^2(\beta_n^{TD} - \delta_n^{TD}) + k(\zeta_{b1} - l)^2\zeta_{b1}^2 - m\zeta_{b1}^2(v_n^{TD})^2 = 0 \quad (17)$$

$$\frac{ml^2(v_{n+1}^{TD})^2 \sin^2(\beta_{n+1}^{TD} - \delta_{n+1}^{TD}) + k(\zeta_{b2} - l)^2\zeta_{b2}^2}{m\zeta_{b2}^2[(v_{n+1}^{TD})^2 + 2gl(\sin(\beta_{n+1}^{TD}) - \sin(\beta_n^{TD}))]} = 1\,. \quad (18)$$

Here, ζ_{b1}, ζ_{b2} represent the distance between the center of mass and the foot placement point when $\dot{\zeta} = 0$. For the point mass system, in which $\zeta = \eta$, this represents the state of maximal spring compression. For consistency, gravity is included in the energy calculation at leg touchdown, but not during the stance phase, in the formulation of $\Delta\psi_2$. Conservation of energy between the start of the first and second stance phases yields $a = (v_n^{TD})^2$, and from equations (7–9), we find $v_{n+1}^{TD}\sin(\beta_{n+1}^{TD} - \delta_{n+1}^{TD}) = v_n^{TD}\sin(\beta_n^{TD} - \delta_n^{TD})$. Substituting these values into the expression for $\Delta\psi_2$ in (15) shows that the integrands of (14-15) are equivalent. Similar arguments can be used to show that equations (17) and (18) are equal, resulting in $\zeta_{b2} = \zeta_{b1}$. By ignoring gravity during stance, we find that $\Delta\psi_1$ necessarily equals $\Delta\psi_2$ such that the period two mapping reduces to

$$v_{n+2}^{TD} = v_n^{TD} \quad (19)$$

$$\delta_{n+2}^{TD} = \delta_n^{TD} \quad (20)$$

$$\beta_{n+2}^{TD} = \beta_n^{TD}\,. \quad (21)$$

Therefore, under these assumptions, this leg touchdown protocol necessarily produces period two gaits. The eigenvalues of the mapping are all unity, indicating that these gaits are neutrally stable. Numerical simulations verify this result for a large number of gaits, even when gravity is included during the stance phase. The limited effect of gravity during the stance phase observed here is restricted to this particular leg touchdown protocol and model. Specifically, this leg touchdown protocol ensures, through conservation of energy and conservation of linear momentum, that orbits of the system are reflection-symmetric about the midpoint of the flight phase. As a result, while angular momentum is not conserved during either stance phase, the net angular impulse delivered by gravity during the first stance phase is counteracted by an equal and opposite net angular impulse during the second stance phase. For

other leg touchdown protocols, especially those relating to period one orbits, gravity can have a significant effect on orbits and orbital stability, as discussed in [8, 18].

Properties of Period one Gaits with $\beta_{n+1}^{TD} = \beta_n^{LO}$

Neutrally stable period one gaits, with $\beta_{n+1}^{TD} = \beta_n^{TD} = \beta_n^{LO}$, exist as a subset of the family of period two gaits analyzed previously. The eigenvalues of the period two mapping in this case represent the square of each eigenvalue in the period one map, suggesting that eigenvalues in the associated period one mapping are ± 1. We pursue a stability analysis in this section to determine if one of the eigenvalues is negative one for this leg touchdown protocol. If an eigenvalue is negative one, then continuity suggests that a leg touchdown protocol exists between the extremes of $\beta_{n+1}^{TD} = \beta_n^{TD}$ and $\beta_{n+1}^{TD} = \beta_n^{LO}$ that produces stable periodic gaits.

The period one Poincaré map for the leg touchdown protocol $\beta_{n+1}^{TD} = \beta_n^{LO}$ is a composition of the stance and flight phase maps. The full stride map is constructed similarly to the period two map, using conservation of energy, conservation of linear momentum and conservation of angular momentum to yield

$$v_{n+1}^{TD} = \sqrt{(v_n^{TD})^2 + 2gl(\sin(\beta_n^{TD}) - \sin(\Delta\psi + \beta_n^{TD}))} \tag{22}$$

$$\delta_{n+1}^{TD} = \pi - \Delta\psi - 2\beta_n^{TD} + \delta_n^{TD} \tag{23}$$

$$\beta_{n+1}^{TD} = \pi - \Delta\psi - \beta_n^{TD} \ . \tag{24}$$

As in [8], consistency requires that we neglect gravity in computing the liftoff velocity in the heading angle map, since gravity is neglected in the computation of the leg sweep angle, $\Delta\psi$, during stance. Neglecting gravity in this computation yields $v_n^{LO} = v_n^{TD}$, resulting in the heading angle map presented above. A period one orbit therefore requires $\Delta\psi = \pi - 2\beta_n^{TD}$, which implies through the stance phase geometry that $\beta_n^{LO} = \beta_n^{TD}$. We construct the Jacobian of the Poincaré map evaluated at the fixed point as

$$\begin{bmatrix} 1 + b\frac{\partial \Delta\psi}{\partial v_n^{TD}} & b\frac{\partial \Delta\psi}{\partial \delta_n^{TD}} & b(2 + \frac{\partial \Delta\psi}{\partial \beta_n^{TD}}) \\ -\frac{\partial \Delta\psi}{\partial v_n^{TD}} & 1 - \frac{\partial \Delta\psi}{\partial \delta_n^{TD}} & -(2 + \frac{\partial \Delta\psi}{\partial \beta_n^{TD}}) \\ -\frac{\partial \Delta\psi}{\partial v_n^{TD}} & -\frac{\partial \Delta\psi}{\partial \delta_n^{TD}} & -1 - \frac{\partial \Delta\psi}{\partial \beta_n^{TD}} \end{bmatrix} \tag{25}$$

where

$$b = \frac{gl\cos(\beta_n^{TD})}{v_n^{TD}} \ . \tag{26}$$

We calculate the eigenvalues of the Jacobian, evaluated at the fixed point, in the Appendix as

$$\lambda_{1,2} = 1 \tag{27}$$

$$\lambda_3 = -1 - \frac{\partial \Delta\psi}{\partial \beta_n^{TD}} - \frac{\partial \Delta\psi}{\partial \delta_n^{TD}} + b\frac{\partial \Delta\psi}{\partial v_n^{TD}} \tag{28}$$

where $\Delta\psi$ is computed as in equation (14).

While ignoring gravity during the stance phase enables $\Delta\psi$ to be computed analytically, as in [14], it results in a complex expression in terms of incomplete elliptic integrals. As in [13], we instead utilize the Schwind-Koditschek approximation [18] to compute $\Delta\psi$ and the associated derivatives. Using this approximation, the computation of $\Delta\psi$ can be approximated by

$$\Delta\psi = \frac{2lv_n^{TD}\sin(\beta_n^{TD} - \delta_n^{TD})(l - \zeta_b)}{\hat{\zeta}\sqrt{((v_n^{TD})^2 - k/m(\hat{\zeta} - l)^2)\hat{\zeta}^2 - l^2(v_n^{TD})^2\sin^2(\beta_n^{TD} - \delta_n^{TD})}} \tag{29}$$

$$\hat{\zeta} = \frac{3\zeta_b + l}{4}\,. \tag{30}$$

While straightforward, computing the derivatives required in the eigenvalue expression is lengthy and left to the Appendix. Using the fixed points computed for the gait family with $\beta_n^{TD} = 1.2$, we numerically compute the third eigenvalue using equation (28) and the relationships for the derivatives detailed in the Appendix. This computation reveals that the third eigenvalue has a maximum deviation of 10% from -1 across all the gaits of the gait family. Purely numerical computation of the Jacobian and associated eigenvalues for each gait reveal that the third eigenvalue is equal to -1 in each case. The difference between the numerical results and our analytical approximation results from neglecting gravity during stance as well as the approximation used for the computation of $\Delta\psi$ and the associated derivatives. However, taken together, these results show that periodic gaits utilizing this leg touchdown protocol are neutrally stable, with one eigenvalue equal to negative one.

4 An Adaptive Control Law

The results of the analyses for the period two and period one orbits under the leg touchdown protocol $\beta_{n+1}^{TD} = \beta_n^{LO}$ are used to guide the construction of an adaptive control law for period one orbits.

4.1 Control of the Point Mass SLIP Model

We begin by deriving a general period one Poincaré map with varying leg touchdown angle, using conservation of energy, conservation of linear momentum during the flight phase, and conservation of angular momentum during the stance phase as

$$v_{n+1}^{TD} = \sqrt{(v_n^{TD})^2 + 2gl(\sin(\beta_n^{TD}) - \sin(\beta_{n+1}^{TD}))} \tag{31}$$

$$\cos(\delta_{n+1}^{TD}) = \sqrt{\frac{(v_n^{TD})^2 + 2gl(\sin(\beta_n^{TD}) - \sin(\beta_n^{LO}))}{(v_n^{TD})^2 + 2gl(\sin(\beta_n^{TD}) - \sin(\beta_{n+1}^{TD}))}}\cos(g(\cdots)) \tag{32}$$

$$\beta_{n+1}^{TD} = f(\beta_n^{TD}, \beta_n^{LO}, v_n^{TD}, \delta_n^{TD}) \tag{33}$$

where

$$g(\beta_n^{TD}, v_n^{TD}, \delta_n^{TD}) = \beta_n^{LO} + \sin^{-1}(\frac{v_n^{TD}}{v_n^{LO}}\sin(\delta_n^{TD} - \beta_n^{TD})) \tag{34}$$

$$\beta_n^{LO} = \pi - \Delta\psi - \beta_n^{TD} \tag{35}$$

$$v_n^{LO} = \sqrt{(v_n^{TD})^2 + 2gl(\sin(\beta_n^{TD}) - \sin(\beta_n^{LO}))}\,. \tag{36}$$

While a period one orbit of the mapping must satisfy $\beta_{n+1}^{TD} = \beta_n^{TD} = \beta_n^{LO}$ and $\Delta\psi = \pi - 2\beta_n^{TD}$, the stability of an orbit depends upon the leg touchdown protocol utilized in response to perturbations from the periodic orbit. Using the fixed angle leg reset policy ($\beta_{n+1}^{TD} = \beta_n^{TD}$) with model parameters similar to those of *Blaberus discoidalis* primarily produces unstable gaits with a single eigenvalue greater than unity, whereas using the leg touchdown protocol $\beta_{n+1}^{TD} = \beta_n^{LO}$ necessarily produces neutrally stable periodic gaits with an eigenvalue of -1. Continuity therefore suggests that the stability of the periodic gait should vary continuously for leg placement protocols between these two extremes. An adaptive control law that incorporates both of these leg touchdown protocols and satisfies the leg angle symmetry condition for a periodic orbit is given by

$$\beta_{n+1}^{TD} = \beta_n^{LO} + c(\beta_n^{TD} - \beta_n^{LO}) \tag{37}$$

where c is an arbitrary constant. Since gait symmetry requires $\beta_n^{TD} = \beta_n^{LO}$ for a periodic gait, c only changes the stability of a gait, since a periodic gait remains periodic for any value of c. In particular, we expect that the unstable gaits observed in the SLIP model will stabilize as c is decreased from unity (the fixed angle leg reset policy, $\beta_n^{TD} = \beta_n^{LO}$), since the unstable eigenvalue must enter the unit circle and tend towards -1 as c tends towards zero (the $\beta_{n+1}^{TD} = \beta_n^{LO}$ protocol).

We investigate the stability properties of periodic gaits utilizing this feedback control law using numerically computed periodic orbits and eigenvalues, with model parameters set to values similar to those of *Blaberus discoidalis*. We begin by analyzing the effect changing c has on the eigenvalues of a representative gait family, as illustrated in Fig. 3. As illustrated in the second panel, decreasing c from unity shifts the non-unity eigenvalue curve downwards, stabilizing an increasing number of gaits until almost all gaits are stabilized for $c = 0.1$. We note, however, that as c decreases, some gaits, while still stable, will be relatively less stable as the eigenvalue determining stability tends towards negative one. This is illustrated in the third panel for a single orbit,

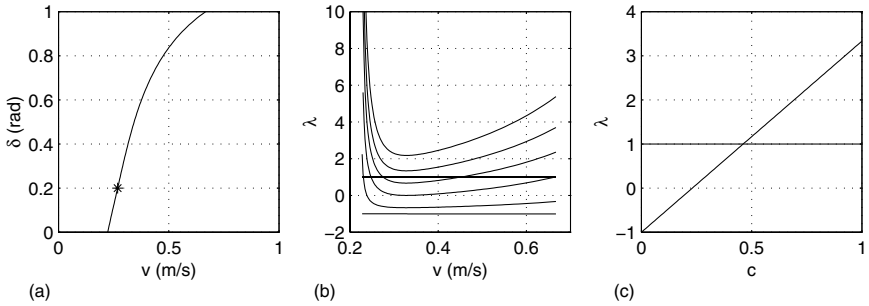

Fig. 3. (**a**) SLIP periodic gait family and stability for $\beta = 1.2$, with other parameters set to those of *Blaberus discoidalis*, as described in the text (**b**) Gait family eigenvalues for $c = 1, 0.7, 0.5, 0.3, 0.1, 0$, with curves moving downwards as c decreases. (**c**) Eigenvalue variation as c varies from 1 to 0 for the periodic gait (*) identified in (a)

denoted with a * in the first panel, where we observe that an almost linear eigenvalue variation occurs with changes in c. As c decreases from unity, the unstable gait becomes less unstable, stabilizes for $c < .46$, and becomes more stable until c reaches 0.23, at which point the eigenvalue begins to grow in magnitude as it approaches -1 at $c = 0$. As c passes through zero, we find that the eigenvalue passes through -1, indicating a flip bifurcation. Therefore, for $c < 0$, we find that the period one orbit once again becomes unstable.

We illustrate the performance of the control law, for $c = 0.3$, in Fig. 4. While a fixed angle leg reset policy is incapable of producing a stable periodic orbit with these model parameters, we see that the inclusion of this simple control law leads to stabilization to a periodic orbit within several stance phases. How quickly a new stable gait is obtained depends upon how close the eigenvalue is to zero, which depends upon c and the model parameters. We note that variations in β^{TD} utilized in stabilizing the orbit remain quite small.

It is important to clarify the definition of asymptotic stability that is being utilized in this context. Since energy conservation and translational invariance naturally produce unity eigenvalues, we apply the definition of asymptotic stability used by Coleman et al. [19] and Coleman and Holmes [20]. In this less restrictive definition of asymptotic stability, a periodic orbit is asymptotically stable if perturbations result in the convergence to a nearby periodic gait. Perturbations to a periodic gait for our system and control result in the attainment of a new, stable gait, due to the partial asymptotic stability of these gaits and the coupling of motions introduced through the inclusion of the control law.

Since the model remains conservative under this control law, we also illustrate the changes in gait stability for a constant energy surface, as illustrated in Fig. 5. The gait family illustrated therein is determined by choosing an en-

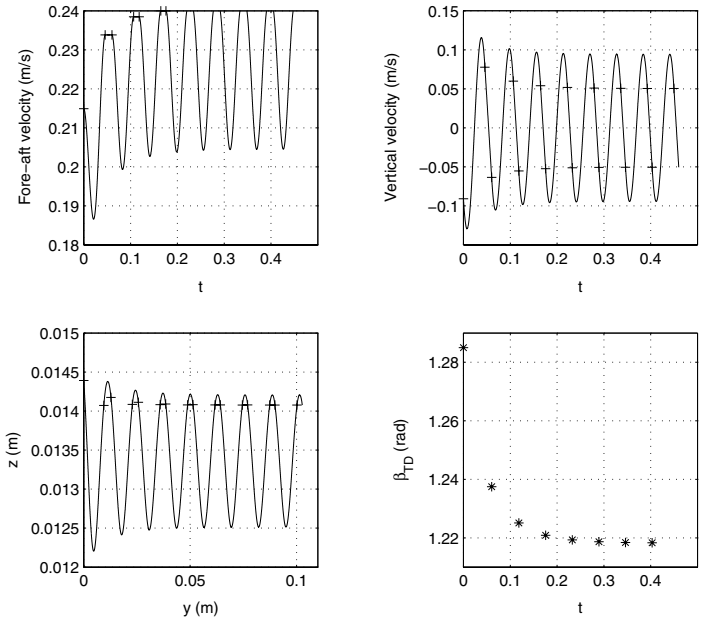

Fig. 4. Stabilization of the SLIP model to a periodic gait for $c = 0.3$, with parameters are set to values similar to the cockroach *Blaberus discoidalis*. *Plus signs* denote the start and end of the stance phase and stars denote the start of the stance phase

ergy value and varying β_n^{TD}, thereby implicitly determining v_n^{TD}, and finding the associated δ_n^{TD} that determines a periodic orbit by a Newton-Raphson iteration. The gaits for this constant energy represent the periodic orbits which the model can settle on, assuming no perturbations occur that change the energy of the system. As c decreases, we see that an increasing number of gaits stabilize, until all gaits are stable at $c = 0.1$. To be clear, however, the definition of asymptotic stability utilized in this work means that perturbations to a particular periodic orbit that do not result in a change in energy do result in the state asymptotically converging to a nearby periodic orbit of the gait family. Obviously, perturbations to a conservative system that result in a change in the total system energy necessarily result in the convergence to a new periodic gait that belongs to a different gait family. Perturbations that would typically be encountered in practice would tend to fall into this latter category rather than the former. In fact, Altendorfer [21] notes that the small range of touchdown speeds evidenced for a constant energy surface necessitates changes in the total system energy if the controlled system is to exhibit a useful range of touchdown velocities.

Achieving asymptotic stability in the more traditional sense to perturbations within the energy surface (i.e. returning to the original periodic orbit) requires a measure of knowledge of the periodic orbit that we wish to stabilize.

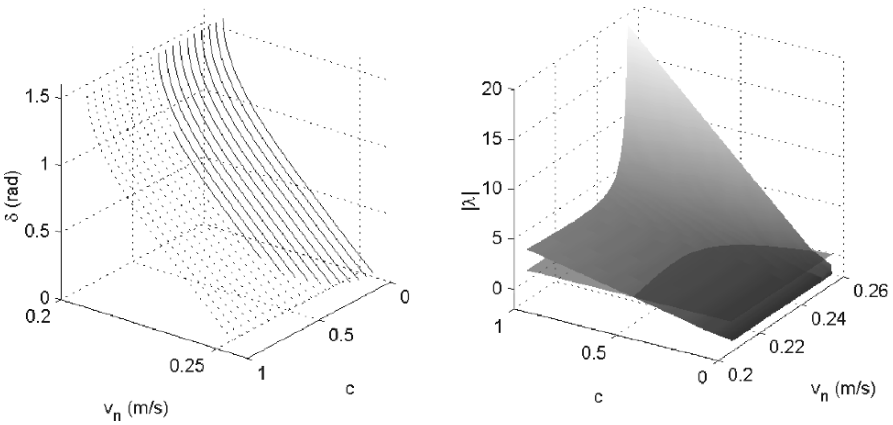

Fig. 5. Periodic gaits and stability for the SLIP model as a function of c, for a constant energy surface corresponding to an insect running at 0.25 m/s at a height of .014 m. All other parameters are similar to those of *Blaberus discoidalis*, as described in the text. (**a**) Periodic gaits for $c = 0.0 - 1.0$, with *dotted* and *solid lines* denoting unstable and stable periodic gaits respectively (**b**) Eigenvalue variation for the periodic gaits of panel (a)

The fixed angle leg reset gaits that exhibit this property for larger animals accomplish this naturally since the leg touchdown protocol defines a desired leg touchdown angle and therefore a desired touchdown velocity, assuming a constant energy. We note that we have constructed a control law similar in structure and content to that presented in this work which includes a dependence on a desired touchdown angle, β_{des}^{TD}. This alternate control law produces asymptotically stable periodic gaits in the more traditional sense, as explained above. The performance of this alternate control law will be investigated in detail in a future work.

Finally, returning to the original gait family plot of Fig. 2, we illustrate how this control law enlarges the basin of attraction, as illustrated in Fig. 6. As c decreases, an increasing number of periodic gaits on all gait family curves stabilize. Considering that perturbations to an orbit will typically occur transverse to the constant energy surface, this control law therefore enables the model to successfully recover from a large range of perturbations. As a result, implementing this control expands the stability basin of the SLIP model.

4.2 Control of the Rigid Body SLIP Model

Displacing the leg attachment point from the center of mass in the SLIP model couples the translational and rotational dynamics and introduces pitching. Use of the same control law formulation, with leg angles defined in the inertial frame, is examined briefly in this section. Preliminary simulations of the rigid body SLIP model suggest that the control law implementation stabilizes

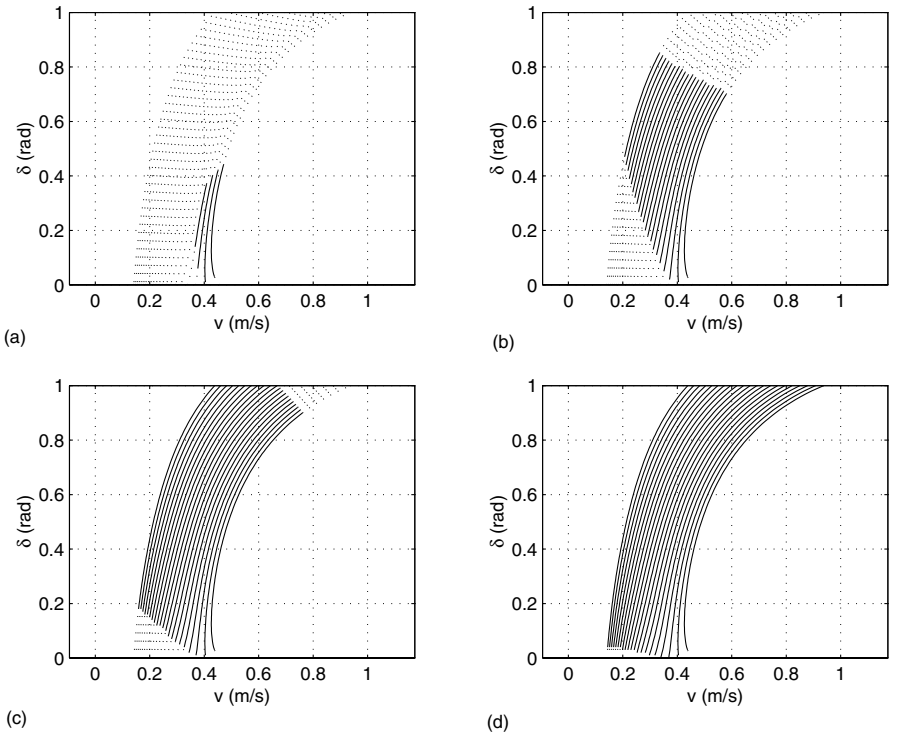

Fig. 6. SLIP gait families for $\beta_n^{TD} = 1.1 - 1.3$ for (**a**) $c = 0.7$ (**b**) $c = 0.5$ (**c**) $c = 0.3$ and (**d**) $c = 0.1$. Gait stability is indicated by *dotted* and *solid lines* for unstable and stable gaits respectively. Model parameters used in calculating the gaits are similar to those of *Blaberus discoidalis*, as described in the text

the system, but does not necessarily produce period one gaits, since the quasi-periodic gaits observed in [8] also appear, as illustrated in Fig. 7. However, the recurrent nature of quasi-periodic orbits enables the use of chaos control methods to enforce stabilization to period one gaits. Specifically, a delay feedback controller [22] is implemented to enforce stabilization to period one orbits. Delay feedback control incorporates the difference between the value of a state variable at one instant and one period delayed, such that the control effect vanishes when the periodic orbit is attained. In our system, delay feedback control is implemented by including a dependence in the control law on the pitch angle as follows

$$\beta_{n+1}^{TD} = \beta_n^{LO} + c(\beta_n^{TD} - \beta_n^{LO}) + c_2(\theta_n^{LO} - \theta_{n-1}^{LO}) \ . \tag{38}$$

The effect of the control law and the control law with delay feedback included is illustrated in Figs. 7 and 8. In both cases, the rigid body SLIP model is simulated from the same set of initial conditions ($v = 0.25$, $\delta = 0.2$, $\theta = 0$, $\dot{\theta} = -0.2$). Figure 7 illustrates that while the inclusion of the leg angle control does

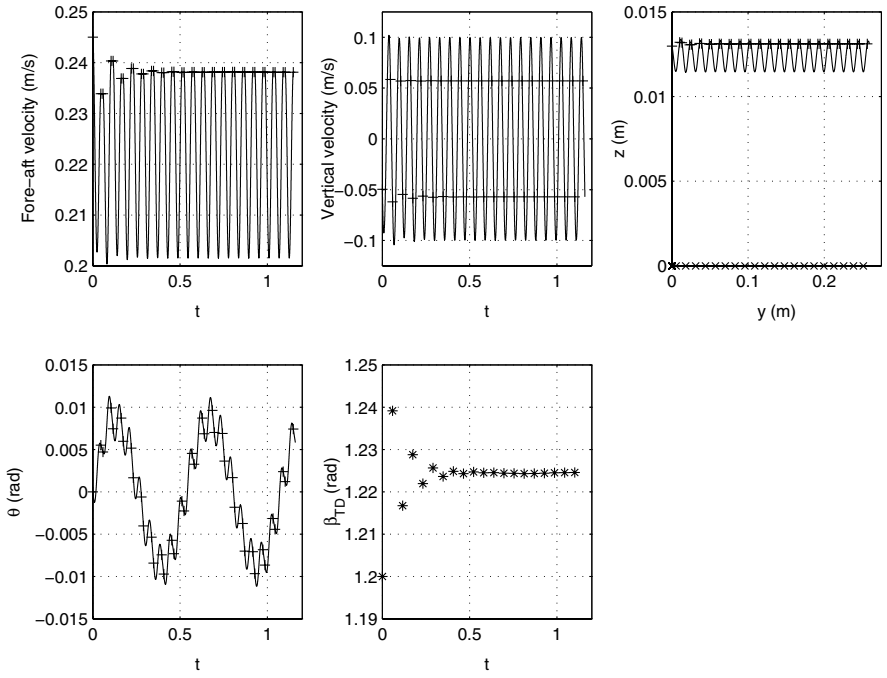

Fig. 7. Rigid body SLIP simulation with the standard leg angle feedback control implemented, with $d = 0.001$, $c = 0.1$, $I = 1.86 \times 10^{-7}$ and initial conditions as specified in the text. Model parameters used in calculating the gaits are similar to those of *Blaberus discoidalis*, as described in the text. *Plus signs* (+) denote the start and end of each stance phase, whereas *stars* (*) denote the start of each stance phase

stabilize the system, the resulting orbit is quasi-periodic rather than period one. While period one gaits may be obtained through the use of this control scheme, they are not necessarily achieved. Conversely, Fig. 8 illustrates the effect of the control law with delay feedback control included. As illustrated, the system not only stabilizes, but stabilizes to a period one orbit. Simulations initiated from a wide range of initial conditions provide similar results. As in previous analyses, the translational and rotational coupling present in the equations of motion, as well as in the control law, lead to the attainment of a new gait in response to perturbations. While further investigation is required to quantify the effects of these control laws on the stability of the rigid body SLIP model, these preliminary results suggest that the control laws presented here will expand the very small basin of attraction identified for this model in previous studies [8].

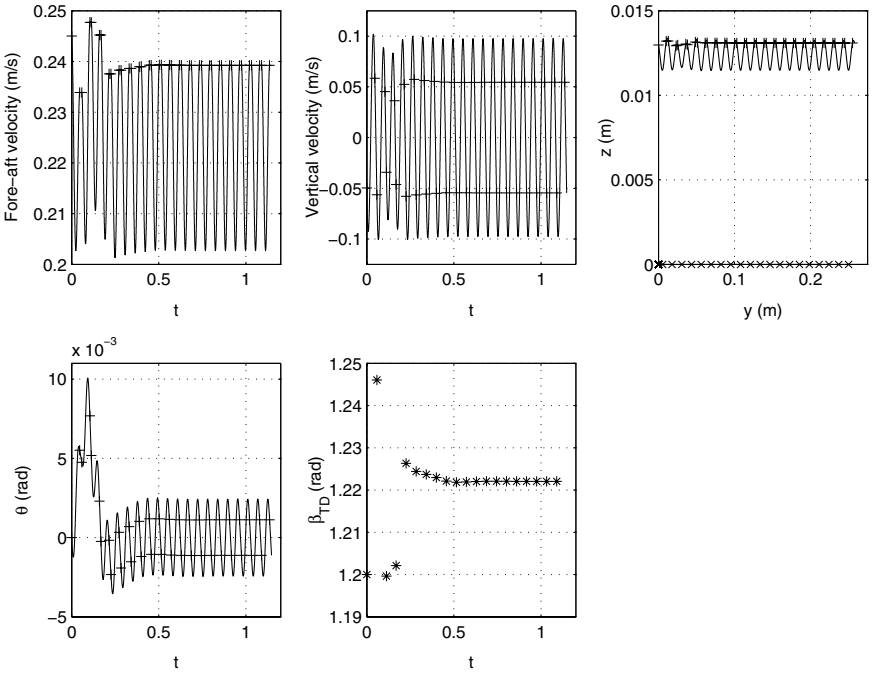

Fig. 8. Rigid body SLIP simulation with delayed feedback control, with $d = 0.001$, $c = 0.1$, $c_2 = 1.25$, $I = 1.86 \times 10^{-7}$ and initial conditions as specified in the text. Model parameters used in calculating the gaits are similar to those of *Blaberus discoidalis*, as described in the text. *Plus signs* (+) denote the start and end of each stance phase, whereas *stars* (*) denote the start of each stance phase

5 Conclusion

In this work, we investigate the applicability of the SLIP model to insect locomotion, specifically that of the cockroach *Blaberus discoidalis*. We find that unlike previous results obtained for the SLIP model when applied to larger animals, periodic gaits produced for these model parameters remain largely unstable over a wide range of leg touchdown angles. This, in conjunction with results indicating that a fixed angle leg reset policy employed in a spatial SLIP model produces only unstable gaits, prompts an investigation into alternate leg touchdown protocols and their effects on gait stability. In particular, we show that a leg angle touchdown protocol that places the next leg down at the previous leg lift-off angle, $\beta_{n+1}^{TD} = \beta_n^{LO}$, necessarily produces neutrally stable period two gaits, and is capable of producing neutrally stable period one gaits with an eigenvalue equal to negative one. Continuity arguments between this leg touchdown protocol and the fixed angle leg reset protocol are used to develop a feedback control law based on inertial leg touchdown angles that stabilizes these unstable periodic gaits. Numerically computed gait families

verify that lowering the parameter c in this control law increases the number of stable periodic gaits, therefore expanding the basin of stability. Implementing the same control law in a rigid body SLIP formulation also produces stable gaits, but not necessarily periodic gaits, since quasi-periodic gaits also appear. Utilizing the pitch angle as delay feedback control in the control law forces stabilization to period one orbits.

The control laws developed in this work are unique in that they: a) do not require knowledge of pre-existing periodic orbits or linearization about those orbits to achieve control b) require relatively simple feedback measurements rather than full state feedback for implementation c) apply control once per stance phase rather than continuously during the stance phase and d) can adapt to perturbations by changing to a different stable periodic gait that is more suitable to the new environment. Qualitatively, it appears that the effectiveness of the control law results from implicit information about the system angular momentum that is present in a reading of the leg lift-off angle. Quantitative exploration of this hypothesis will be conducted in future work. Additionally, it appears that these control laws may also have applicability in both the horizontal plane and spatial SLIP models. Preliminary simulations utilizing two control laws specifying the leg placement angles of a point mass spatial SLIP model appear to, at least for some parameter ranges, produce stable periodic gaits. We plan to investigate these applications further in later works.

References

[1] R. Blickhan. The spring-mass model for running and hopping. *J. Biomechanics*, 11/12:1217–1227, 1989.

[2] R. Blickhan and R.J. Full. Similarity in multi-legged locomotion: bouncing like a monopode. *J. Comp. Physiol. A*, 173:509–517, 1993.

[3] G.A. Cavagna, N.C. Heglund, and C.R. Taylor. Mechanical work in terrestrial locomotion: two basic mechanisms for minimizing energy expenditure. *Am. J. Physiol.*, 233 (5):R243–R261, 1977.

[4] T.A. McMahon and G.C. Cheng. The mechanics of running: how does stiffness couple with speed? *J. Biomechanics*, 23 (suppl 1):65–78, 1990.

[5] R.J. Full and M.S. Tu. Mechanics of a rapid running insect: two-, four- and six-legged locomotion. *J. Exp. Biol.*, 156:215–231, 1991.

[6] C.T. Farley, J. Glashenn, and T.A. McMahon. Running springs: speed and animal size. *J. Exp. Biol.*, 185:71–86, 1993.

[7] R.J. Full, R. Blickhan, and L.H. Ting. Leg design in hexpedal runners. *J. Exp. Biol.*, 158:369–390, 1991.

[8] R. Ghigliazza, R.M. Altendorfer, P. Holmes, and D. Koditschek. A simply stabilized running model. *SIAM Journal on Applied Dynamical Systems*, 2(2):187–218, 2003.

[9] A. Seyfarth, H. Geyer, M. Gunther, and R. Blickhan. A movement criterion for running. *J. of Biomechanics*, 35:649–655, 2002.

[10] A. Seyarth, H. Geyer, and H. Herr. Swing-leg retraction: a simple control model for stable running. *J. Exp. Biology*, 206:2547–2555, 2003.
[11] J. Seipel and P. Holmes. Running in three dimensions: analysis of a point-mass sprung-leg model. *Intl. J. Robotics Research*, 24(8), 2005.
[12] A. Ruina. Non-holonomic stability aspects of piecewise holonomic systems. *Reports on Mathematical Physics*, 42(1/2):91–100, 1998.
[13] J. Schmitt and P. Holmes. Mechanical models for insect locomotion: Stability and parameter studies. *Physica D*, 156(1–2):139–168, 2001.
[14] J. Schmitt and P. Holmes. Mechanical models for insect locomotion: Dynamics and stability in the horizontal plane – Theory. *Biological Cybernetics*, 83(6):501–515, 2000.
[15] J. Schmitt and P. Holmes. Mechanical models for insect locomotion: Dynamics and stability in the horizontal plane – Application. *Biological Cybernetics*, 83(6):517–527, 2000.
[16] J. Guckenheimer and P. Holmes. *Nonlinear Oscillations, Dynamical Systems, and Bifurcations of Vector Fields*. Springer-Verlag, New York, NY, 1990.
[17] L.H. Ting, R. Blickhan, and R.J. Full. Dynamic and static stability in hexapedal runners. *J. Exp. Biol.*, 197:251–269, 1994.
[18] W.J. Schwind and D.E. Koditschek. Approximating the stance map of a 2 dof monoped runner. *J. Nonlinear Science*, 10(5):533–568, 2000.
[19] M. Coleman, A. Chatterjee, and A. Ruina. Motions of a rimless spoked wheel: a simple 3d system with impacts. *Dynamics and stability of systems*, 12(3):139–169, 1997.
[20] M. Coleman and P. Holmes. Motions and stability of a piecewise holonomic system: the discrete chaplygin sleigh. *Regul. Chaotic Dyn.*, 4:55–77, 1999.
[21] R. Altendorfer, R. Ghigliazza, P. Holmes, and D. Koditschek. Exploiting passive stability for hierarchical control. In *Proceedings of the Fifth International Conference on Climbing and Walking Robots (CLAWAR 2002)*, pp. 81–85, London, 2002. Professional Engineering Publishing Limited.
[22] K. Pyragas. Continuous control of chaos by self-controlling feedback. *Phys. Lett. A*, 170:421–428, 1992.

Appendix

The eigenvalues of the period one Poincaré map are determined from $\det(\lambda I - DP)$, where I is the identity matrix and DP is the Jacobian matrix of (25). Evaluating the determinant and simplifying yields

$$\begin{aligned}&(\,\lambda - 1 - b\frac{\partial \Delta\psi}{\partial v_n^{TD}})(\lambda^2 + (\frac{\partial \Delta\psi}{\partial \beta_n^{TD}} + \frac{\partial \Delta\psi}{\partial \delta_n^{TD}})\lambda - 1 - \frac{\partial \Delta\psi}{\partial \beta_n^{TD}} - \frac{\partial \Delta\psi}{\partial \delta_n^{TD}}) + \\ &(\,\lambda - 1)b\frac{\partial \Delta\psi}{\partial v_n^{TD}}\frac{\partial \Delta\psi}{\partial \delta_n^{TD}} + (\lambda - 1)(2 + \frac{\partial \Delta\psi}{\partial \beta_n^{TD}})b\frac{\partial \Delta\psi}{\partial v_n^{TD}} = 0\,. \qquad \text{(A-1)}\end{aligned}$$

Factoring a $(\lambda - 1)$ out of all terms yields

$$(\lambda - 1)((\lambda - 1 - b\frac{\partial \Delta\psi}{\partial v_n^{TD}})(\lambda + 1 + \frac{\partial \Delta\psi}{\partial \beta_n^{TD}} + \frac{\partial \Delta\psi}{\partial \delta_n^{TD}}) + b\,\frac{\partial \Delta\psi}{\partial \delta_n^{TD}}\frac{\partial \Delta\psi}{\partial v_n^{TD}} + 2b\frac{\partial \Delta\psi}{\partial v_n^{TD}} + b\frac{\partial \Delta\psi}{\partial \beta_n^{TD}}\frac{\partial \Delta\psi}{\partial v_n^{TD}}) = 0\ . \tag{A-2}$$

Expanding further and simplifying yields

$$(\lambda - 1)^2(\lambda + 1 + \frac{\partial \Delta\psi}{\partial \beta_n^{TD}} + \frac{\partial \Delta\psi}{\partial \delta_n^{TD}} - b\frac{\partial \Delta\psi}{\partial v_n^{TD}}) = 0 \tag{A-3}$$

which yields the expression for the eigenvalues in (27–28).

From (28), it is clear that we need to calculate $\frac{\partial \Delta\psi}{\partial \beta_n^{TD}}$, $\frac{\partial \Delta\psi}{\partial v_n^{TD}}$, $\frac{\partial \Delta\psi}{\partial \delta_n^{TD}}$, in order to determine the value for the relevant eigenvalue that determines stability. The approximation of $\Delta\psi$ presented in (29–30) can be simplified further as

$$\Delta\psi = \frac{p}{q} \tag{A-4}$$

$$p = 128 l v_n^{TD} \sin(\beta_n^{TD} - \delta_n^{TD})(l - \zeta_b) \tag{A-5}$$

$$q = (3\zeta_b + l)\sqrt{s} \tag{A-6}$$

$$s = (16(v_n^{TD})^2 - \frac{9k}{m}(\zeta_b - l)^2)(3\zeta_b + l)^2 - 256 l^2 (v_n^{TD})^2 \sin^2(\beta_n^{TD} - \delta_n^{TD})\ . \tag{A-7}$$

Since $\Delta\psi$ is a function of ζ_b, in evaluating the required partial derivatives, we need $\frac{\partial \zeta_b}{\partial v_n^{TD}}$, $\frac{\partial \zeta_b}{\partial \delta_n^{TD}}$, $\frac{\partial \zeta_b}{\partial \beta_n^{TD}}$, all of which may be determined implicitly from (17) as

$$\frac{\partial \zeta_b}{\partial v_n^{TD}} = \frac{m v_n^{TD}(\zeta_b^2 - l^2 \sin^2(\beta_n^{TD} - \delta_n^{TD}))}{\zeta_b(-m(v_n^{TD})^2 + k(2\zeta_b - l)(\zeta_b - l))} \tag{A-8}$$

$$\frac{\partial \zeta_b}{\partial \delta_n^{TD}} = \frac{m l^2 (v_n^{TD})^2 \sin(2(\beta_n^{TD} - \delta_n^{TD}))}{2\zeta_b(-m(v_n^{TD})^2 + k(2\zeta_b - l)(\zeta_b - l))} \tag{A-9}$$

$$\frac{\partial \zeta_b}{\partial \beta_n^{TD}} = -\frac{m l^2 (v_n^{TD})^2 \sin(2(\beta_n^{TD} - \delta_n^{TD}))}{2\zeta_b(-m(v_n^{TD})^2 + k(2\zeta_b - l)(\zeta_b - l))}\ . \tag{A-10}$$

Given these partial derivatives, we can calculate the expressions for the required derivatives of $\Delta\psi$ from the quotient rule

$$\frac{\partial \Delta\psi}{\partial ()} = \frac{q\dot{p} - p\dot{q}}{q^2} \tag{A-11}$$

where () represents $v_n^{TD}, \delta_n^{TD}, \beta_n^{TD}$ and $\dot{()}$ denotes derivatives with respect to these variables, which can be expressed as

$$\frac{\partial p}{\partial v_n^{TD}} = 128 l \sin(\beta_n^{TD} - \delta_n^{TD})((l - \zeta_b) - v_n^{TD}\frac{\partial \zeta_b}{\partial v_n^{TD}}) \tag{A-12}$$

$$\frac{\partial p}{\partial \delta_n^{TD}} = -128 l v_n^{TD}(\cos(\beta_n^{TD} - \delta_n^{TD})(l - \zeta_b) + \frac{\partial \zeta_b}{\partial \delta_n^{TD}} \sin(\beta_n^{TD} - \delta_n^{TD})) \quad \text{(A-13)}$$

$$\frac{\partial p}{\partial \beta_n^{TD}} = 128 l v_n^{TD}(\cos(\beta_n^{TD} - \delta_n^{TD})(l - \zeta_b) - \frac{\partial \zeta_b}{\partial \beta_n^{TD}} \sin(\beta_n^{TD} - \delta_n^{TD})) \quad \text{(A-14)}$$

and

$$\frac{\partial q}{\partial v_n^{TD}} = 3\frac{\partial \zeta_b}{\partial v_n^{TD}}\sqrt{s} + \frac{(3\zeta_b + 1)(t\frac{\partial \zeta_b}{\partial v_n^{TD}} + w - u\sin(\beta_n^{TD} - \delta_n^{TD}))}{\sqrt{s}} \quad \text{(A-15)}$$

$$\frac{\partial q}{\partial \delta_n^{TD}} = 3\frac{\partial \zeta_b}{\partial \delta_n^{TD}}\sqrt{s} + \frac{(3\zeta_b + 1)(t\frac{\partial \zeta_b}{\partial \delta_n^{TD}} - x\frac{\partial \zeta_b}{\partial \delta_n^{TD}} + u v_n^{TD}\cos(\beta_n^{TD} - \delta_n^{TD}))}{\sqrt{s}} \quad \text{(A-16)}$$

$$\frac{\partial q}{\partial \beta_n^{TD}} = 3\frac{\partial \zeta_b}{\partial \beta_n^{TD}}\sqrt{s} + \frac{(3\zeta_b + 1)(t\frac{\partial \zeta_b}{\partial \beta_n^{TD}} - x\frac{\partial \zeta_b}{\partial \beta_n^{TD}} - u v_n^{TD}\cos(\beta_n^{TD} - \delta_n^{TD}))}{\sqrt{s}} \quad \text{(A-17)}$$

where

$$t = 6(3\zeta_b + l)(16(v_n^{TD})^2 - \frac{9k}{m}(\zeta_b - l)^2) \quad \text{(A-18)}$$

$$u = 512 l^2 v_n^{TD}\sin(\beta_n^{TD} - \delta_n^{TD}) \quad \text{(A-19)}$$

$$w = (32 v_n^{TD} - \frac{18k}{m}(\zeta_b - l)\frac{\partial \zeta_b}{\partial v_n^{TD}})(3\zeta_b + l)^2 \quad \text{(A-20)}$$

$$x = \frac{18k}{m}(\zeta_b - l)(3\zeta_b + 1)^2\ . \quad \text{(A-21)}$$